Available online at www.sciencedirect.com

ScienceDirect

journal homepage: www.elsevier.com/locate/he

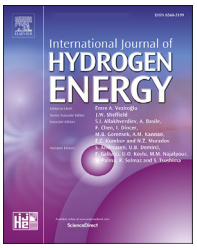

The semiconductor $SrFe_{0.2}Ti_{0.8}O_{3-\delta}$-ZnO heterostructure electrolyte fuel cells

Muhammad Ali Kamran Yousaf Shah [a], *Naveed Mushtaq* [b], *Sajid Rauf* [b], *Chen Xia* [b,c,**], *Bin Zhu* [a,b,*]

[a] *Engineering Research Center of Nano-Geo Materials of Ministry of Education, Department of Materials Science and Chemistry, China University of Geosciences, 388 Lumo Road, Wuhan, 430074, China*

[b] *Hubei Collaborative Innovation Center for Advanced Organic Chemical Materials, Faculty of Physics and Electronic Science, Hubei University, Wuhan, Hubei, 430062, China*

[c] *Department of Energy Technology, KTH Royal Institute of Technology, Stockholm, SE, 10044, Sweden*

HIGHLIGHTS

- SFT-ZnO heterostructure composite was developed as SOFC electrolyte.
- SFT-ZnO achieved high ionic conductivity of 0.21 S cm^{-1} at 520 °C.
- Fuel cell-based on SFT-ZnO demonstrated high performance.
- Bulk-heterojunction effect of SFT-ZnO was studied to interpret its high fuel cell performance.

ARTICLE INFO

Article history:
Received 24 July 2019
Received in revised form
12 September 2019
Accepted 18 September 2019
Available online 21 October 2019

Keywords:
Solid oxide fuel cell
Semiconductor heterostructure
$SrFe_{0.2}Ti_{0.8}O_{3-\delta}$-ZnO
High performance
Bulk-p-n heterojunction effect

ABSTRACT

Highly ion-conducting properties in heterostructure composites and semiconductors have drawn significant attention in recent years for developing new electrolytes in low-temperature solid oxide fuel cells (LT-SOFCs). In this work, a new semiconductor heterostructure composite $SrFe_{0.2}Ti_{0.8}O_{3-\delta}$ (SFT)-ZnO consisting of p-type SFT and n-type ZnO is proposed and evaluated as an electrolyte in LT-SOFCs. Electrochemical studies reveal that the prepared SFT-ZnO is a mixed ion-electron conductor possessing a high ionic conductivity of 0.21 S cm^{-1} at 520 °C and the assembled SFT-ZnO fuel cell can achieve a favorable peak power output of 650 mW cm^{-2} along with high open-circuit voltage (OCV) of 1.06 V at 520 °C. By referring the semiconductor conduction types and energy band parameters of SFT and ZnO, a p-n bulk-heterojunction effect is proposed to describe the electronic blocking and ionic promotion processes of SFT-ZnO electrolyte in a fuel cell. Our work suggests a new insight into the design of effective LT-SOFC electrolytes by using semiconductor heterostructure material.

© 2019 Hydrogen Energy Publications LLC. Published by Elsevier Ltd. All rights reserved.

* *Corresponding author*. Engineering Research Center of Nano-Geo Materials of Ministry of Education, Department of Materials Science and Chemistry, China University of Geosciences, 388 Lumo Road, Wuhan, 430074, China.

** *Corresponding author*. Hubei Collaborative Innovation Center for Advanced Organic Chemical Materials, Faculty of Physics and Electronic Science, Hubei University, Wuhan, Hubei, 430062, China.

E-mail addresses: cxia@kth.se (C. Xia), binzhu@kth.se, binzhu@cug.com (B. Zhu).

https://doi.org/10.1016/j.ijhydene.2019.09.145

0360-3199/© 2019 Hydrogen Energy Publications LLC. Published by Elsevier Ltd. All rights reserved.

Introduction

Fast ionic transport is highly desired by solid oxide fuel cells (SOFCs) as high ionic conduction in electrolytes and electrodes is directly linked to rapid fuel cell start-up, favorable power outputs and long endurance [1–3]. Specifically, it is required a sufficient ionic conductivity of >0.1 S cm^{-1} in electrolyte materials to guarantee excellent fuel cell performance. Yttria-stabilized zirconia $(Y_2O_3)_x$ $(ZrO_2)_{1-x}$ (YSZ) and rare-earth-doped CeO_2 are the most frequently used electrolytes in SOFCs, due to their ionic conducting capability compared to other common ionic oxides in addition to chemical compatibility with electrodes [4]. However, since that superior ionic conductivity is a thermally motivated process, which determines the high requirements of these typical electrolytes concerning to working temperature, current SOFCs' always demand high operational temperatures of over 800 °C. This leads to long start-up and shut-down cycles, high material and technological costs, and fast performance degradation rates [1–5]. Therefore, enabling high ionic conduction in electrolytes at low operational temperatures, mainly 300–500 °C, is a vital prerequisite for optimization of SOFC technology from performance, cost, and stability perspective.

To reach this target, extensive efforts have been dedicated to improving O^{2-} conductivity in doped CeO_2 system, H^+ conductivity in proton conductors, and dual O^{2-}/H^+ conductivity in composite materials by defect modulation, thin-film techniques, and structural design in the past decades [6–10]. Among these studies, oxide heterostructures constructed by semiconductor and ionic conductor is of great notice. A typical example is YSZ/$SrTiO_3$ (STO) planar heterostructure, ultrathin YSZ sandwiched by STO layers reported by Garcia-Barriocanal et al., and nanocolumn YSZ on STO film matrix reported by Shinbuhm Lee et al. [10,11]. It was indicated that the heterostructure gained remarkably improved O^{2-} conductivity compared with bulk YSZ. This behavior has also been detected by Sang Mo Yang et al. in a heterostructure of Sm-doped CeO_2 (SDC) nanocolumns embedded in STO matrix, which revealed enhanced ionic conductivity by one order of magnitude than that of plain SDC [12]. More importantly, all these heterostructures demonstrated excellent ionic conductivity at low temperatures of 300–500 C. Garcia-Barriocanal et al. ascribed the enhancement of ionic conductivity to the atomic reconstruction at interface region, which provided plenty of carriers and a high-mobility plane for ions. Where after, such 2D planar semiconductor-ionic conductor heterostructure was further elaborately modified by virtue of nanocomposite approach into 3D homogeneous bulk-heterostructure and was applied into SOFC with the successful demonstration [13–19]. For instance, bulk-heterostructure made of $La_{0.6}Sr_{0.4}Co_{0.2}Fe_{0.8}O_{3-\delta}$ (LSCF) and Sm/Ca co-doped CeO_2 (SCDC) in the form of homogenous composite. The LSCF-SCDC indicated a high ionic conductivity of over 0.1 S cm^{-1} at >500 °C as a result of interfacial conduction, and presented an open circuit voltage (OCV) above 1.0 V and maximum power density of 1080 mW cm^2 at 550 °C along with good durability when sandwiched between symmetrical electrodes of $Ni_{0.8}Co_{0.15}Al_{0.05}LiO_{2-\delta}$ (NCAL) to construct fuel cell [14–16]. In conclusion, these studies of semiconductor-ionic conductor heterostructures offer a prospect for enabling low-temperature (LT) operation of SOFCs at below 500 °C and suggest that semiconductors can play a crucial role to promote the ion-conducting ability in ionic conductors via hetero-interface effects.

In parallel, semiconductors themselves have also been developed as alternative electrolytes for SOFCs based on different mechanisms [20–27]. A breakthrough study reported by Zhou et al. showed that perovskite semiconductor $SmNiO_3$ (SNO) could obtain high ionic conductivity induced by hydrogen incorporation, which can compare with best-performing solid electrolytes. The SNO can be used as an electrolyte in a simple configuration of Pt/SNO/Pt, delivering considerable power density of 225 mW cm^{-2} at 500 °C. The electronic conduction of SNO was suppressed through the Mott transition caused by spontaneous hydrogen incorporation, which discriminates the new working principle of SNO electrolyte from conventional electrolytes [20]. In another report, Tao et al. reported a decent proton conductivity (0.1 S cm^{-1} at 500 °C) in a layer-structured semiconductor $Li_xAl_{0.5}Co_{0.5}O_2$ (LCAO) because of H^+ injection in-situ into the LCAO lattice to form H-LCAO for H^+ transportation, resulting in a fuel cell performance of 173 mW cm^{-2} at 525 °C [21]. Our previous work also investigated the feasibility of a typical versatile semiconductor ZnO for SOFC electrolyte use. The studied ZnO electrolyte can enable a decent fuel cell power densities of 158–482 mW cm^{-2} at 450–550 °C [22]. Recently, Dong et al. presented a design of energy band alignment using a thin film of TiO_2 semiconductor as an electrolyte and achieved high fuel cell performance of 364 mW cm^{-2} along with open-circuit voltage (OCV) of 1.1 V [28]. Chen et al. studied a core-shell perovskite La–$SrTiO_3$, unveiling that this semiconductor electrolyte can reach a super high ionic conductivity of 0.221 S cm^{-1} at 550 °C and achieve marvelous fuel cell performance of 908 mW cm^{-2} [29]. Besides, there are some other promising perovskite semiconductors that own considerable ionic conduction, even though they have not yet been evaluated in SOFC as an electrolyte. For instance, it is pointed out that a redox stable perovskite $SrFeO_{3-\delta}$ can gain increased oxygen vacancies by doping of Ti on the B site, yielding an excellent ionic conductivity [24]. These findings manifest that semiconductor itself holds great potential as LT electrolyte regardless of its current insufficient cell performance.

By reviewing the above studies and taking advantages of bulk-heterostructure and semiconductor electrolytes, this paper aims at developing a new bulk-heterostructure electrolyte for LT-SOFC application based on two semiconductor phases SFT and ZnO. Our investigations include: i) prepare bulk-heterostructure samples of SFT-ZnO using sol-gel methods and fabricate the corresponding SOFC devices based on SFT-ZnO; ii) identify the feasibility of SFT-ZnO as an effective electrolyte in LT-SOFC; iii) characterization and electrochemical analysis of the prepared materials and devices. According to these experimental results, the properties of SFT-ZnO are compared with previous heterostructure and semiconductor electrolytes, and the effects of semiconductor bulk-heterojunction that benefits SOFC performance are further investigated, on the basis of which, our approach of all-semiconductor bulk-heterostructure is

established, as a new strategy to develop advanced electrolytes for LT-SOFCs.

Experimental segment

A stoichiometric amount of $Sr(NO_3)_3$ (Sigma Aldrich 99.99%) and $Fe(NO_3)_3$ (Sigma Aldrich 99.99%) were mixed and dissolved into de-ionized water to form homogenous solution under continuous stirring. Afterward, an appropriate molar ratio of liquid TiO_2 (Sigma Aldrich 99.99%) was added into the above solution, followed by adding citric acid as a gelating agent. Afterward, the solution was continuously stirred at 60 °C until the gel was obtained. Subsequently, the resulting gel was dried at 200 °C in an electric oven for 10 h and was further sintered in a furnace at 900 °C for 4 h at 3 °C/min, followed by grinding to attain homogenous and well-grinded powder. Finally, to prepare the SFT-ZnO composite materials, commercial zinc oxide (ZnO) (Sigma Aldrich 99.9%) was blended with the as-prepared powder with a 1:1 mass ratio and grounded adequately again to get a homogenous composite powder for characterizations and cell fabrication.

Electrodes were prepared based on commercially purchased $Ni_{0.8}Co_{0.15}Al_{0.05}LiO_2$ (NCAL) (Tianjin Bamo Science and Technology Joint Stock Limited Tianjin, China) and Ni-foam. The used NCAL-Ni electrodes in this study were made by mixing NCAL powders with terpineol solvent in an appropriate ratio to get slurry, which was then pasted on Ni foam following by desiccation at 120 °C for 1 h to form NCAL-Ni for both electrode and current collector uses. Two fuel cell pellets were fabricated using SFT and SFT-ZnO composite as an electrolyte layer, respectively. The pellets were constructed by pressing the appropriate amount of electrolyte material between two Ni-NCAL electrodes under the load of 200–220 MPa. The configuration of fabricated two cells was NCAL/SFT-ZnO/NCAL, and NCAL/SFT/NCAL is ~1.5 mm in thickness and 13 mm in diameter, with an active area of 0.64 cm^{-2}. Afterward, these two cells were sintered at 650 °C for 1 h before the performance measurement. Such sintering temperature is determined for the reason that our devices are operated at low temperatures (420–520 °C) and too high temperature may cause the oxidation of Ni-foam, which will deteriorate the structure of NCAL-Ni electrode and the current collection ability of Ni. Finally, silver was applied on both sides of the cell pellet for fuel cell performance measurements.

By utilizing a Bruker D-8 advanced x-ray diffractometer (XRD, Burker Corporation, Germany) of Cu K alpha radiations (λ=1.54060 nm), the crystal structure of samples was examined at 45 kV, 40 mA of tube voltage and current, respectively. The XRD pattern was obtained in the 2θ range of between 20 and 80° and was refined by JADE 6.5. The Field emission scanning electron microscopy (FESEM) (FESEM, JEOL JSM7100F Japan) was utilized to study the sample morphology and cross-sectional view of the fabricated fuel cell devices. Ultraviolet photoelectron spectroscopy (UPS) (ESCALAB 250XI, Thermo Fisher Scientific UK) were employed to attain valance band maximum with He–I (21.2eV) as a source energy instrumental resolution source of about 100 meV, and UV–visible was engaged to obtain the absorption spectra. Impedance analysis was carried out utilizing Gammaray reference 3000 instruments to obtain the impedance spectra under OCV mode and frequency dependency (~0.1 Hz–1 MHz) to study electrical and electrochemical properties of the composite electrolyte. The obtained EIS data was further fitted with an equivalent circuit using ZSIMPWIN software. The I–V and I–P characteristic were performed via IT8511 electronic load (ITECH Electrical Co., Ltd., China) at 420–520 °C under the gas operation of (120–150 mL/min) hydrogen as a fuel and ambient air as an oxidant respectively.

Results and discussion

Crystalline structure and morphology

Fig. 1(a) shows the XRD patterns of SFT ($SrF_{0.2}Ti_{0.8}O_{3-\delta}$), ZnO, and SFT-ZnO heterostructure. The main diffraction peaks of SFT are located at 2θ of 25, 32, 39, 46, 57, 68, and 76° and well-indexed to (012), (110), (111), (210), (211), (220) and (310) planes, corresponded to a typical cubic perovskite structure (JCPDS File No. 33-0677). While the characteristic diffraction peaks of ZnO are located at 2θ of 31, 34, 36 47, 56, 62, 67 and 68 and can be identified as the (100), (002), (101), (102), (110), (103) and (112) planes with hexagonal wurtzite structure of ZnO [22,24]. However, the crystal structure of SFT-ZnO composite shows the diffraction peaks of two different phases that can clearly be identified as individual SFT and ZnO, indicating the coexistence of SFT and ZnO in as prepared heterostructure composite. There is no extra peak observed in the patterns, eliminating the possibility of chemical reaction forming new phases between the SFT and ZnO phases. Besides, the crystalline size calculated using the Debye Scherrer formula [30] for SFT and ZnO is around 48 nm and 26 nm, respectively.

Fig. 1(b–d) show the morphology of the prepared SFT, commercial ZnO, and the resulting SFT-ZnO powders characterized by scanning electron microscopy (SEM), respectively. The SFT particles exhibit irregular shape with size ranging from hundred nanometers to around 1 μm, while the ZnO present nano-sized and micro-sized columnar grains and particles. Furthermore, the SFT-ZnO heterostructure composite gains improved morphology, revealing a uniform distribution of the two phases (SFT and ZnO) as shown in the SEM image (Fig. 1(d)). The particles of SFT-ZnO are well connected with one another, which helps in the high rate of oxygen permeation. Due to such feature, the as-prepared composite fulfills the essential requirement for electrolyte membranes by building continuous interfaces and channels for charge transport, and create more active sites for electrochemical reaction.

Fuel cell performance

The single SFT and SFT-ZnO heterostructure composite were applied as electrolytes in SOFCs, respectively, and fuel cell performances were measured at low temperatures of 420–520 °C. Fig. 2(a) and (b) and describe the obtained current-voltage (I–V) characteristics and the corresponding current-power (I–P) plots for SFT and SFT-ZnO electrolyte fuel cells, separately. It has shown that both SFT and SFT-ZnO heterostructure can realize excellent electrolyte functionality, exhibiting favorable current density, and high OCVs. The SFT

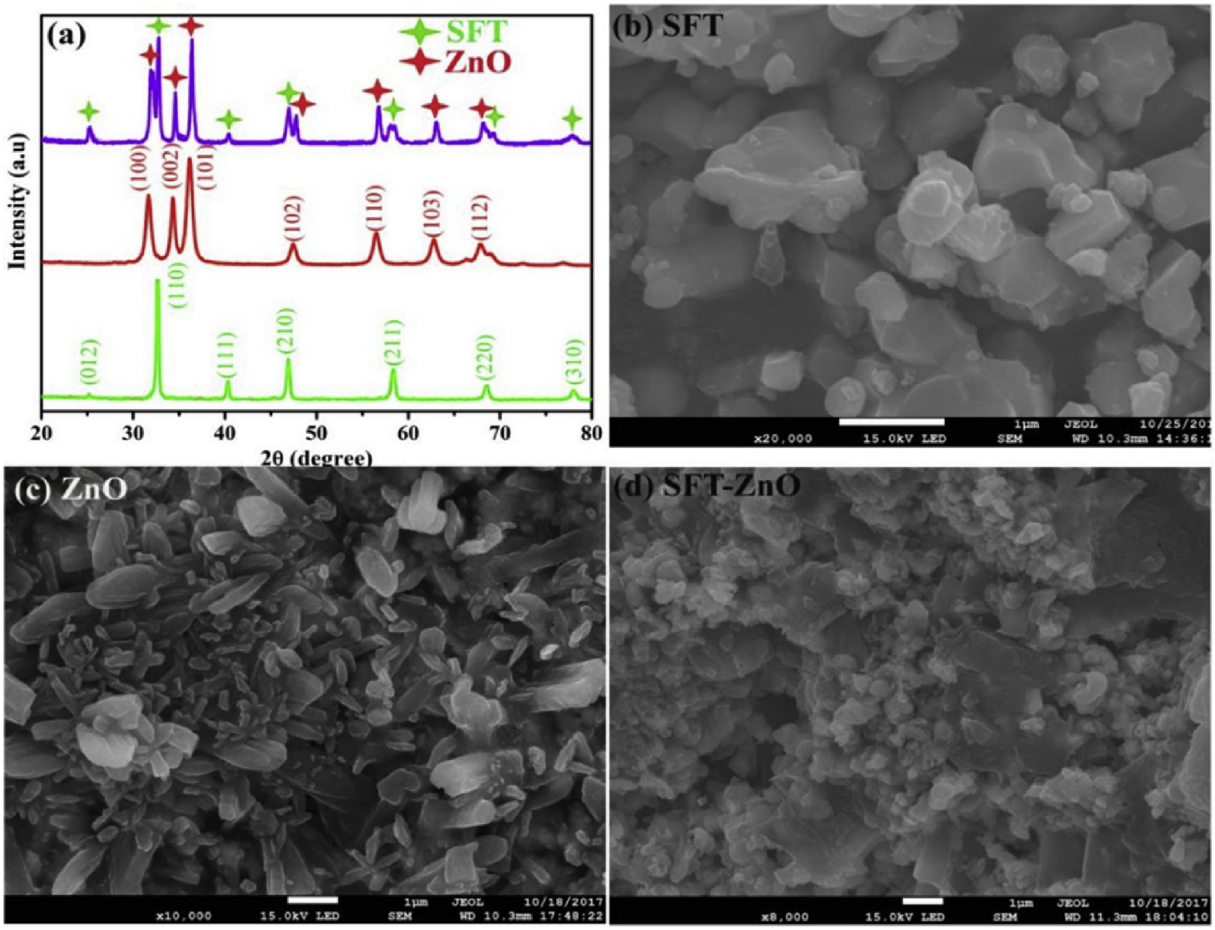

Fig. 1 – (a) X-ray diffraction pattern of the prepared $SrFe_{0.2}Ti_{0.8}O_{3-\delta}$ (SFT), ZnO and SFT-ZnO heterostructure; (b–d) SEM images for SFT, ZnO and SFT-ZnO heterostructure, respectively.

electrolyte fuel cell delivers a maximum power density of 320 mW cm^{-2} with an OCV of 1.05 V at 520 °C, which is surpassing the reported results for semiconductor electrolytes SNO and LCAO [20,21]. Such high OCV can attribute to a Schottky barrier of the Schottky junction formed between anodic metallic Ni and semiconductor SFT, which is able to prevent the electrons from pass through the anode/electrolyte interface [31]. Besides, as reported, the SFT can gain significantly enhanced ionic conductivity through doping of low- and intermediate-concentration of Fe into $SrTiO_3$, which can support fast ionic transport in the SFT electrolyte layer [32]. More attractively, the SFT-ZnO electrolyte fuel cell demonstrates remarkably enhanced performance as compared to SFT fuel cell, exhibiting peak power density of 650 mW cm^{-2} with high OCV of 1.06 V at 520 °C and manifests a capability of low-temperature operation with power outputs of 90–450 mW cm^{-2} at 370–470 °C.

Fig. 2(c) gives a typical cross-sectional SEM image of the SFT-ZnO fuel cell device after the operation. It clearly shows the intermediate layer of SFT-ZnO that sandwiched between two NCAL-Ni electrodes. Fig. 2(d) further presents the magnified view of the anodic NCAL-Ni/SFT-ZnO interface in Fig. 2(d), displaying the porous structure of the anode layer and dense structure of SFT-ZnO layer, which guarantees the effective electrode reaction, sufficient OCVs, and high ionic transport (current density) of the fuel cell.

Electrochemical and electrical analysis

To investigate the electrochemical and electrical properties of SFT-ZnO heterostructure, impedance spectra of SFT-ZnO fuel cells were measured in H_2/air atmosphere at 420, 470, and 520 °C. Fig. 3 presents the Nyquist plots of the measured EIS data, which were further fitted to an equivalent circuit, as shown in Fig. 3(a) and (b) and . The acquired EIS curves describe three dominant processes represented by intersects at high frequencies (HF), at intermediate frequency and at low frequencies (LF) regions, representing ohmic resistance R_o, charge transfer resistance R_1 and mass transfer resistance R_2, respectively. It can be found that both SFT cell and SFT-ZnO cell have small ohmic resistances at 420–520 °C, but the later reveals much lesser polarization resistance, signifying the fast charge transfer and mass transfer processes [33–35]. According to the fitted R_o from EIS, the total electrical conductivity of SFT-ZnO consisting of both ionic and electronic contributions can be calculated by the following equation:

$$\sigma = \frac{L}{R \times S}$$

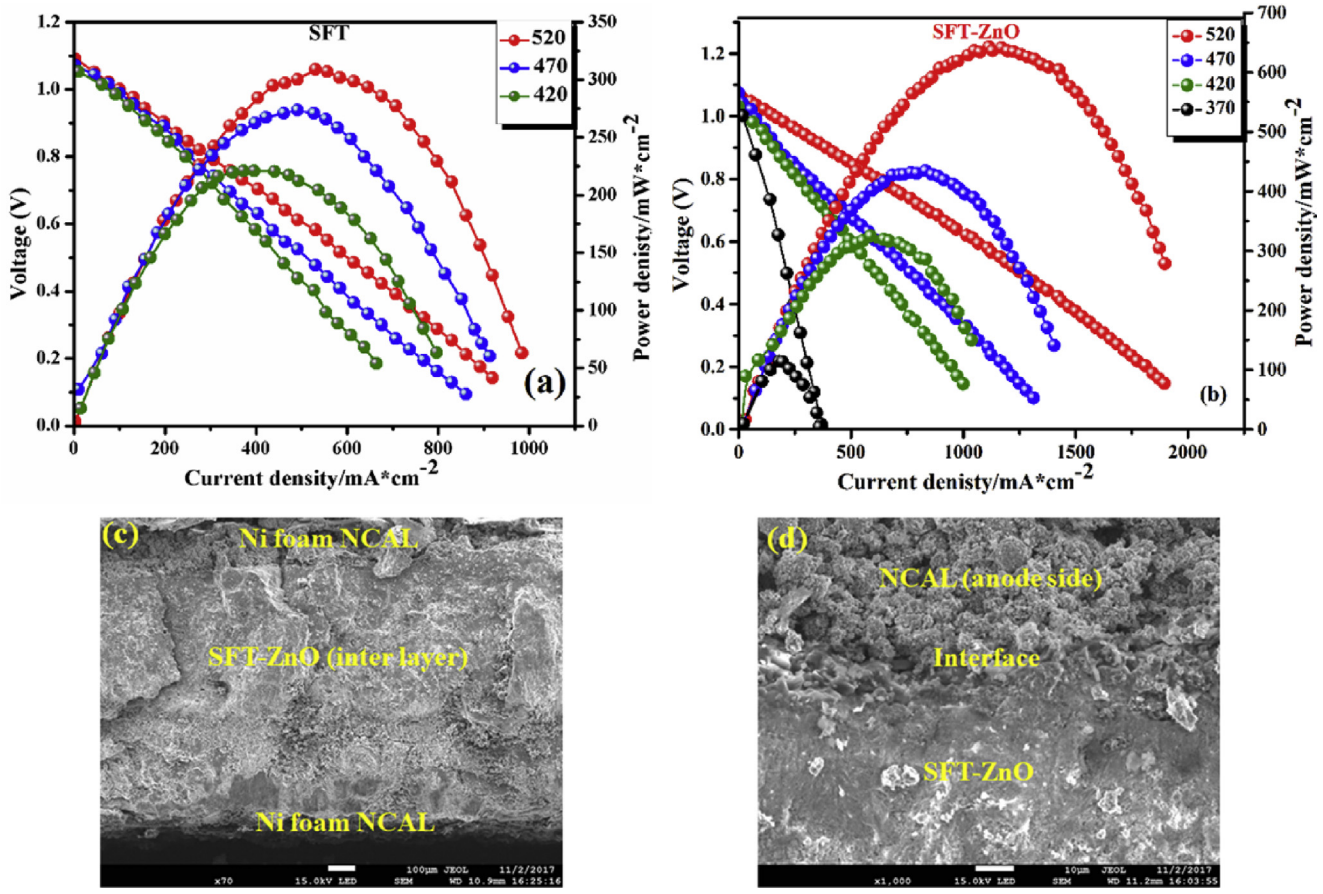

Fig. 2 – Fuel cell performances of measurements (a) for SFT, (b) for SFT-ZnO as the electrolytes at different temperature 370–520 °C (c) cross-sectional SEM image of the cell with SFT-ZnO heterostructure electrolyte and (d) NCAL and SFT-ZnO interface magnified the view of the cell.

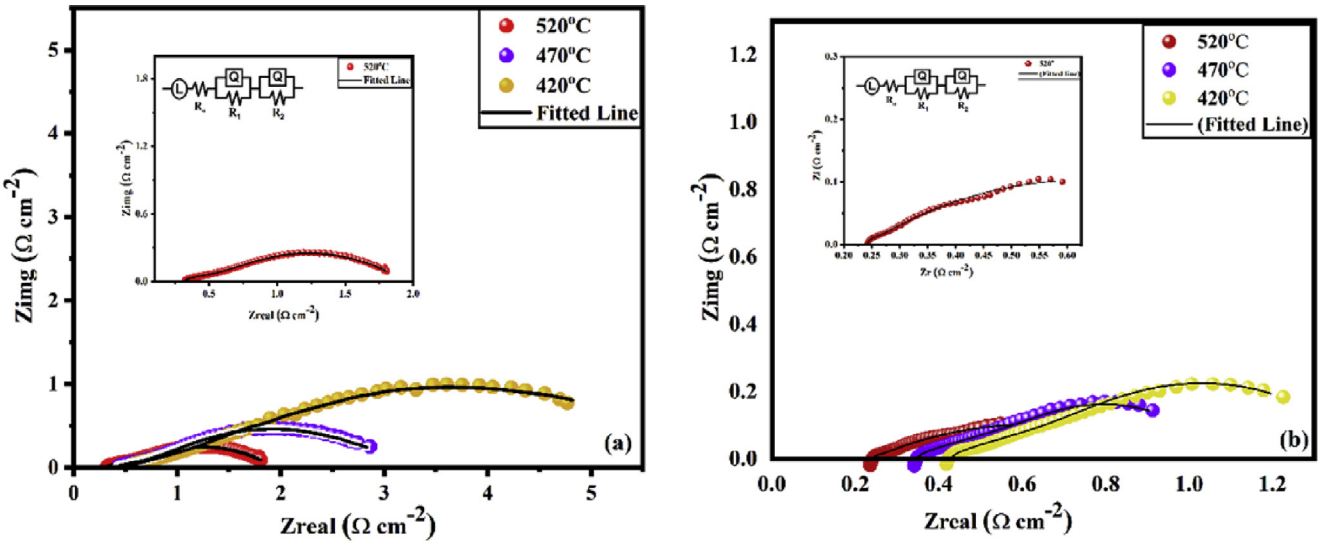

Fig. 3 – Impedance spectra of cell (a) SFT, (b) SFT-ZnO with an electrode NCAL at a different temperature, Impedance circuit are used to fit the impedance spectra of the symmetrical cell.

In which, L shows the thickness of the electrolyte membrane layer, and S is the effective area. Besides, the capacitance has been calculated using the following equation:

$$C_i = \frac{(R_i \times Q_i)^{\frac{1}{n}}}{R_i}$$

Table 1 – Shows the EIS fitted data of SFT obtain using ZSIMPWIN software.

Composition SFT	Inductance (L)	R_o Ωcm^{-2}	R_1 Ωcm^{-2}	Q_1(CPE)	n	C_1	R_2 Ωcm^{-2}	Q_2(CPE)	n	C_2
520 °C	1.73E-8	0.3355	0.4168	0.5905	0.2013	2.933	1.0647	1.286	0.4976	2.5806
470 °C	1.074E-8	0.4362	0.6009	0.604	0.1992	3.036	1.8459	1.303	0.5003	2.6127
420 °C	1.07E-8	0.5444	0.6546	0.5926	0.2015	2.940	3.582	1.270	0.4969	2.5918

Table 2 – Shows the EIS fitted data of SFT-ZnO obtain using ZSIMPWIN software.

Composition SFT-ZnO	Inductance (L)	R_o Ωcm^{-2}	R_1 Ωcm^{-2}	Q_1(CPE)	N	C_1	R_2 Ωcm^{-2}	Q_2(CPE)	n	C_2
520 °C	8.319E-8	0.2301	0.0846	0.003488	0.9877	0.00469	0.2801	1.891	0.3289	5.906
470 °C	5.552E-8	0.3269	0.1745	1.043	0.745	1.404	0.4103	3.156	0.8268	3.823
420 °C	5.477E-8	0.402	0.2569	1.533	0.3094	0.8303	0.5721	0.8041	0.2956	2.7213

Where the R is the resistance, and Q is the constant phase element has the unit of Ω cm^{-2} and F cm$^{-2,}$ respectively. The fitted data of SFT and SFT-ZnO is depicted in below Tables 1 and 2.

Furthermore, the ionic resistance of SFT-ZnO can be estimated from the slope of the linear part in the polarization curve (Fig. 2(b)), as that the linear part in the central region reflects ohmic polarization which corresponds to the resistance of ionic flow in the electrolyte and electronic flow in electrodes, and most ohmic polarization results from the ionic resistance in electrolyte [36]. Thus, the ionic conductivity of SFT-ZnO is obtained, achieving a high value of 0.21 S cm^{-1} at 520 °C, as plotted with its total conductivity in Fig. 4, which is superior to the reported results of typical intermediate-temperature electrolytes such as SDC/Na_2CO_3 [37,38]. The corresponding activation energy for the ionic conductivity of SFT-ZnO can be calculated by the following equation:

$$\sigma = \frac{A}{T}\exp\left(-\frac{E_a}{kT}\right)$$

where T is the absolute temperature, A is an exponential factor, and k is Boltzmann constant. The obtained activation energy for ionic conduction is about 0.7 eV. These results reflect that by forming a p-n heterostructure, the SFT-ZnO composite can gain improved fuel cell performance, enhanced ionic conductivity, and low activation energy, which suggests that the designed heterostructure has a promotion mechanism on ionic transport [39].

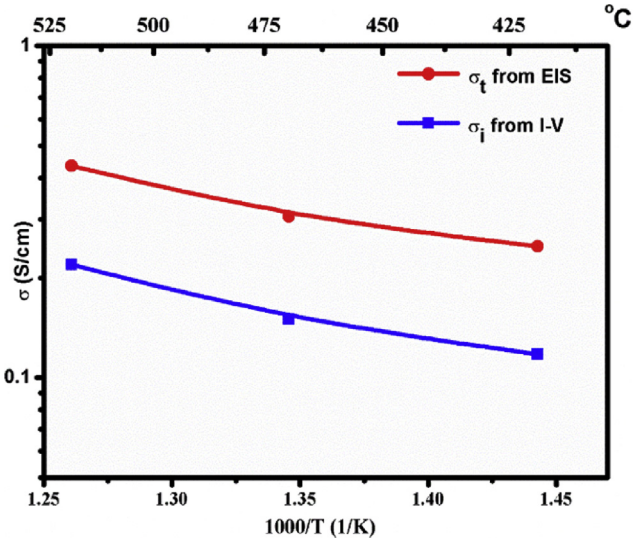

Fig. 4 – Total and ionic conductivities of SFT-ZnO as a function of 1000/T at 420–520 °C.

Also worth noting is that the electronic conductivity of SFT-ZnO can be obtained via subtracting the ionic conductivity from total one, reaching an almost identical value (0.22 S cm^{-1}) as that of ionic conductivity at 520 °C. This implies that the SFT-ZnO is a mixed ion-electron conductor, while its electronic conduction can be effectively suppressed under fuel cell conduction through an electron blocking mechanism so that the fuel cell can achieve high OCVs. Since, the heterostructure composite is made of p-type and n-type semiconductors, it is speculated that the ionic promotion mechanism and electronic blocking mechanism are both owing to a p-n heterojunction effect between SFT and ZnO nanoparticles, which might establish gradient energy band and built-in electric field to facilitate ionic transport and prevent electrons from passing through [40,41].

Energy band levels and p-n heterojunction effect

To certify above surmise, energy levels of SFT and ZnO are of great concern. Therefore, UV–vis absorption and UPS analysis were performed for SFT and ZnO, separately [42]. Fig. 5(a) and (b) display the UV–vis absorbance spectra of SFT and ZnO with clear absorption edges, from which, the band gaps of SFT and ZnO can be calculated using the following relation [43,44].

$$\alpha h\nu = A\left(h\nu - E_g\right)^n$$

Where α is the absorption coefficient, $h\nu$ is the energy of photons; A is the constant and n is 1/2 for direct bandgap semiconductor [45]. The resultant band gaps for SFT, ZnO, and SFT-ZnO are 2.60, 3.10 and 2.9 eV, respectively. The bandgap of SFT is in accordance with the previous result by reported Wu et al., which indicated that the bandgap of $SrTiO_3$ is about 3.25 eV and after doping with iron oxide (SFT) the bandgap reduced to around 2.61 eV [46]. Based on UPS results depicted in Fig. 5(c) and (d), the valence band (VB) maxima can be determined as 7.30 and 9.40 eV for SFT and ZnO, respectively, according to the following equation:

$$Valence\ band = h\nu - (SC - V_{VBE})$$

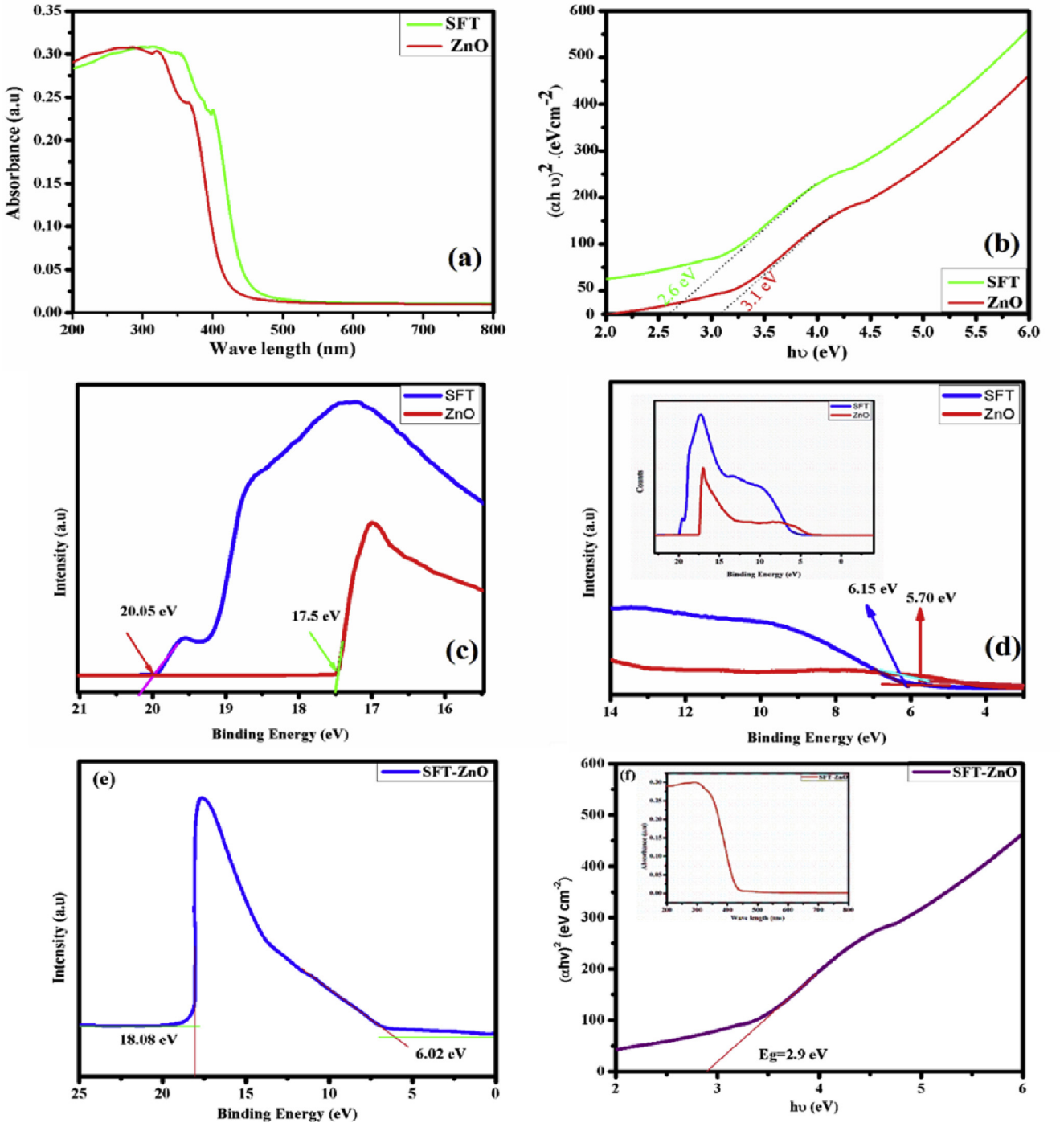

Fig. 5 – (a) UV–visible absorbance spectra and (b) bandgap view of SFT and ZnO; (c) High energy intercept and (d) low energy intercept of the UPS for SFT and ZnO; (e, f) Ups and UV–visible spectra for SFT-ZnO.

where hv is the incident He source of energy 21.2 eV, V_{VBE} represents the energy difference between the Fermi level and VBM edge and SC represent a secondary cutoff edge. Combined with bandgap results, the conduction band (CB) levels can be attained as 4.70 eV for SFT and 6.3 eV ZnO. The VB and CB for composite SFT-ZnO lie between the SFT and ZnO as can be derived from Fig. 5(e).

Since SFT and ZnO possess diverse energy band level parameters, when SFT and ZnO particles contact to create heterophasic interfaces, their different Fermi energy levels will even up to reach a continuous state at the interface region. In this way, the SFT and ZnO can form a p-n bulk-heterojunction at particle scale in the composite. To clearly describe the junction effect on electrochemical enhancement (ionic

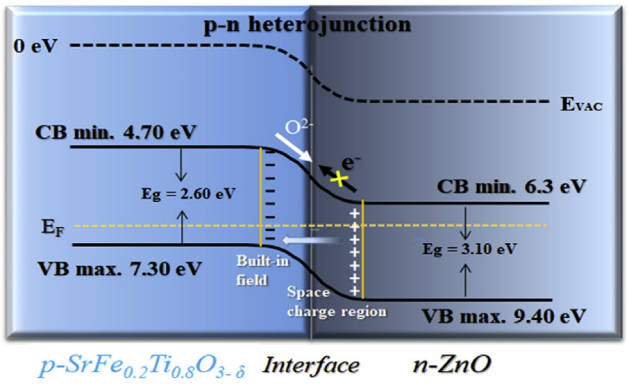

Fig. 6 – Energy band structure of SFT-ZnO p-n heterojunction and the proposed mechanism for ionic promotion and electronic blocking.

promotion) and charge separation (electron-blocking) process, the energy band alignment of SFT-ZnO p-n junction is schematically illustrated in Fig. 6.

Generally, in a p-n junction, positive and negative charges redistribute at the interface of p/n semiconductors to constitute a built-in field (space charge region) [47,48]. In the case of SFT-ZnO p-n bulk-heterojunction, on the one hand, the electric field was able to prevent electrons from passing through, resulting in suppressed electronic conduction throughout the SFT/ZnO interface; on the other hand, oxygen ions could be motivated and accelerated by the electrostatic force to gain enhanced conductivity, improved the OCV and lowered activation energy [49]. Based on this mechanism, the higher power density of SFT-ZnO cell as compared to SFT cell can be reasonably interpreted: the ionic enhancement process mainly took place at the grain boundary interface between SFT and ZnO. Thus the grain-boundary ionic resistance would be reduced and led to a high grain-boundary ionic conductivity of SFT-ZnO. Besides, the electronic blocking behavior was only restricted in the heterostructure electrolyte layer, and would not occur at the electrolyte/electrode interface, which means that sufficient electrons can participate in the electrode reaction and result in a small polarization resistance. These benefits induced by the p-n heterojunction effect thus guaranteed the high fuel cell OCV and electrochemical performance of SFT-ZnO fuel cell.

Conclusions

In this work, a semiconductor heterostructure SFT-ZnO has been successfully prepared via the sol-gel method and applied as an electrolyte in LT-SOFC. The fuel cell-based on SFT-ZnO electrolyte delivered the highest power density 650 mW cm^{-2} and high OCV 1.06 V at low temperature of 520 °C, superior to that of the fuel cell based on single SFT electrolyte, unveiling a favorable electrolyte functionality. Our investigation found that the developed SFT-ZnO heterostructure possesses significantly high ionic conductivity of 0.21 S cm^{-1} at 520 °C along with activation energy 0.7 eV. Furthermore, the electrochemical property of SFT-ZnO was studied via impedance spectra measurements. The higher performance of SFT-ZnO fuel cell that compared to SFT fuel cell was discovered to be mainly because of the small ohmic and polarization resistances. A conceivable mechanism based on energy band alignment was proposed to demonstrate electron obstruction and ionic enhancement processes. Our study demonstrates that semiconductor-based electrolytes in the form of heterostructure can make a significant contribution and impact on developing new electrolyte materials and next-generation advanced LT-SOFC.

Acknowledgment

This work was supported by the National Natural Science Foundation of China (NSFC, grant Nos. 51774259, 51772080 and, 51675496), Engineering Research Center of Nano-Geo Materials of Ministry of Education (NGM2017KF004, NGM2017KF012, and NGM2018KF016).

REFERENCES

[1] Skinner SJ, Kilner JA. Oxygen ion conductors. Mater Today 2003;6:30–7.
[2] Wachsman ED, Lee KT. Lowering the temperature of solid oxide fuel cells. Science 2011;334:935–9.
[3] Ormerod RM. Solid oxide fuel cells. Chem Soc Rev 2003;32:17–28.
[4] Rivera A, Santamaria J, Leon C. Electrical conductivity relaxation in thin-film yttria-stabilized zirconia. Appl Phys Lett 2001;78:610–2.
[5] Wachsman E, Ishihara T, Kilner J. Low-temperature solid-oxide fuel cells. MRS Bull 2014;39:773–9.
[6] Leon C, Santamaria J, Boukamp BA. Oxide interfaces with enhanced ion conductivity. MRS Bull 2013;38:1056–63.
[7] Zuo C, Zha S, Liu M, Hatano M, Uchiyama M. $Ba(Zr_{0.1}Ce_{0.7}Y_{0.2})O_{3-\delta}$ as an electrolyte for low-temperature solid-oxide fuel cells. Adv Mater 2006;18:3318–20.
[8] Zhu B, Fan L, Lund P. Breakthrough fuel cell technology using ceria-based multi-functional nanocomposites. Appl Energy 2013;106:163–75.
[9] Huang H, Nakamura M, Su P, Fasching R, Saito Y, Prinz FB. High-performance ultrathin solid oxide fuel cells for low-temperature operation. J Electrochem Soc 2007;154:B20–4.
[10] Garcia-Barriocanal J, Rivera-Calzada A, Varela M, Sefrioui Z, Iborra E, Leon C, Pennycook SJ, Santamaria J. Colossal ionic conductivity at interfaces of epitaxial ZrO_2: Y_2O_3/$SrTiO_3$ heterostructures. Science 2008;321:676–80.
[11] Lee S, Zhang W, Khatkhatay F, Wang H, Jia Q, MacManus-Driscoll JL. Ionic conductivity increased by two orders of magnitude in micrometer-thick vertical yttria-stabilized ZrO2 nanocomposite films. Nano Lett 2015;15:7362–9.
[12] Yang SM, Lee S, Jian J, Zhang W, Lu P, Jia Q, et al. Strongly enhanced oxygen ion transport through samarium-doped CeO_2 nanopillars in nanocomposite films. Nat Commun 2015;6:8588.
[13] Zhu B, Raza R, Abbas G, Singh M. An electrolyte-free fuel cell constructed from one homogenous layer with mixed conductivity. Adv Funct Mater 2011;21:2465–9.
[14] Wang B, Wang Y, Fan L, Cai Y, Xia C, Liu Y, et al. Preparation and characterization of Sm and Ca co-doped

ceria–$La_{0.6}Sr_{0.4}Co_{0.2}Fe_{0.8}O_{3-\delta}$ semiconductor–ionic composites for electrolyte-layer-free fuel cells. J Mater Chem A 2016;4:15426–36.
[15] Wang B, Cai Y, Xia C, Kim J-S, Liu Y, Dong W, et al. Semiconductor-ionic membrane of lasrcofe-oxide-doped ceria solid oxide fuel cells. Electrochim Acta 2017;248:496–504.
[16] Zhu B, Wang B, Wang Y, Raza R, Tan W, Kim J-S, et al. Charge separation and transport in La0. $6Sr_{0.4}Co_{0.2}Fe_{0.8}O_{3-\delta}$ and ion-doping ceria heterostructure material for new generation fuel cell. Nano Energy 2017;37:195–202.
[17] Zhu B, Raza R, Qin H, Liu Q, Fan L. Fuel cells based on electrolyte and non-electrolyte separators. Energy Environ Sci 2011;4:2986–92.
[18] Dong X, Tian L, Li J, Zhao Y, Tian Y, Li Y. Single layer fuel cell based on a composite of $Ce_{0.8}Sm_{0.2}O_{2-\delta}$–$Na_2CO_3$ and a mixed ionic and electronic conductor $Sr_2Fe_{1.5}Mo_{0.5}O_6$. J Power Sources 2014;249:270–6.
[19] Fan L, Zhu B, Su P-C, He C. Nanomaterials and technologies for low temperature solid oxide fuel cells: recent advances, challenges and opportunities. Nano Energy 2018;45:148–76.
[20] Zhou Y, Guan X, Zhou H, Ramadoss K, Adam S, Liu H, et al. Strongly correlated perovskite fuel cells. Nature 2016;534:231.
[21] Lan R, Tao S. Novel proton conductors in the layered oxide material $Li_{x1}Al_{0.5}Co_{0.5}O_2$. Adv Energy Mater 2014;4. 1301683.
[22] Xia C, Qiao Z, Feng C, Kim J-S, Wang B, Zhu B. Study on zinc oxide-based electrolytes in low-temperature solid oxide fuel cells. Materials 2017;11:40.
[23] Suwanboon S, Amornpitoksuk P, Haidoux A, Tedenac JC. Structural and optical properties of undoped and aluminium doped zinc oxide nanoparticles via precipitation method at low temperature. J Alloy Comp 2008;462:335–9.
[24] Mushtaq N, Xia C, Dong W, Abbas G, Raza R, Ali A, et al. Perovskite $SrFe_{1-x}Ti_xO_{3-\delta}$ (x<= 0.1) cathode for low temperature solid oxide fuel cell. Ceram Int 2018;44:10266–72.
[25] Li L, Zhu B, Zhang J, Yan C, Wu Y. Electrical properties of nanocube CeO_2 in advanced solid oxide fuel cells. Int J Hydrogen Energy 2018;43:12909–16.
[26] Liu Y, Wu Y, Zhang W, Zhang J, Wang B, Xia C, et al. Natural $CuFe_2O_4$ mineral for solid oxide fuel cells. Int J Hydrogen Energy 2017;42:17514–21.
[27] Liu L, Liu Y, Li L, Wu Y, Singh M, Zhu B. The composite electrolyte with an insulation Sm_2O_3 and semiconductor NiO for advanced fuel cells. Int J Hydrogen Energy 2018;43:12739–47.
[28] Dong W, Tong Y, Zhu B, Xiao H, Wei L, Huang C, et al. Semiconductor TiO 2 thin film as an electrolyte for fuel cells. J Mater Chem A 2019;7:16728–34.
[29] Chen G, Zhu B, Deng H, Luo Y, Sun W, Liu H, et al. Advanced fuel cell based on perovskite La–SrTiO3 semiconductor as the electrolyte with superoxide-ion conduction. ACS Appl Mater Interfaces 2018;10:33179–86.
[30] Yokokawa H, Kawada T, Dokiya M. Thermodynamic regularities in perovskite and K_2NiF_4 compounds. J Am Ceram Soc 1989;72:152–3.
[31] Zhu B, Lund PD, Raza R, Ma Y, Fan L, Afzal M, et al. Schottky junction effect on high performance fuel cells based on nanocomposite materials. AdvEnergy Mater 2015;5. 1401895.
[32] Gao H, Liu J, Chen H, Li S, He T, Ji Y, et al. The effect of Fe doping on the properties of SOFC electrolyte YSZ. Solid State Ion 2008;179:1620–4.
[33] He W, Wu X, Yang G, Shi H, Dong F, Ni M. $BaCo_{0.7}Fe_{0.22}Y_{0.08}O_{3-\delta}$ as an active oxygen reduction electrocatalyst for low-temperature solid oxide fuel cells below 600°C. ACS Energy Lett 2017;2:301–5.
[34] Duan C, Tong J, Shang M, Nikodemski S, Sanders M, Ricote S, et al. Readily processed protonic ceramic fuel cells with high performance at low temperatures. Science 2015;349:1321–6.
[35] Xia C, Mi Y, Wang B, Lin B, Chen G, Zhu B. Shaping triple-conducting semiconductor $BaCo_{0.4}Fe_{0.4}Zr_{0.1}Y_{0.1}O_{3-\delta}$ into an electrolyte for low-temperature solid oxide fuel cells. Nat Commun 2019;10:1707.
[36] Xia C, Qiao Z, Shen L, Liu X, Cai Y, Xu Y, et al. Semiconductor electrolyte for low-operating-temperature solid oxide fuel cell: Li-doped ZnO. Int J Hydrogen Energy 2018;43(28):12825–34.
[37] Pai Y-Y, Tylan-Tyler A, Irvin P, Levy J. Physics of $SrTiO_3$-based heterostructures and nanostructures: a review. Rep Prog Phys 2018;81. 036503.
[38] Raza R, Ahmad MA, Iqbal J, Akram N, Gao Z, Javed S, et al. $Ce_{0.8}(SmZr)_{0.2}O_2$-carbonate nanocomposite electrolyte for solid oxide fuel cell. Int J Energy Res 2014;38:524–9.
[39] Ullah MK, Ahmad N, Khan SU-D, Alvi F, Abbas G, Rafique A, et al. Structural and electrochemical studies of microwave sintered nanocomposite electrolytes for solid oxide fuel cells. Int J Hydrogen Energy 2019;44:10964–70.
[40] Wang H, Zhang L, Chen Z, Hu J, Li S, Wang Z, et al. Semiconductor heterojunction photocatalysts: design, construction, and photocatalytic performances. Chem Soc Rev 2014;43:5234–44.
[41] Zheng Y, Zhou T, Zhao X, Pang WK, Gao H, Li S, et al. Atomic interface engineering and electric-field effect in ultrathin Bi_2MoO_6 nanosheets for superior lithium ion storage. Adv Mater 2017;29. 1700396.
[42] Xue F, Huang J, Li T, Wang Z, Zhou X, Wei L, et al. Lowering the synthesis temperature of Y_3 Fe_5O_{12} by surfactant assisted solid state reaction. J Magn Magn Mater 2018;446:118–24.
[43] Azimi M, seyed Sadjadi M, Farhadyar N. Fabrication and characterization of core/shell ZnO/gold nanostructures" and study of their structural and optical properties". Orient J Chem 2016;32:2517–23.
[44] Singh S, Chakrabarti P. Effect of mesa structure formation on the electrical properties of zinc oxide thin film transistors. J Nanosci Nanotechnol 2014;14:3552–6.
[45] Singh S, Kumar Y, Kumar H, Vyas S, Periasamy C, Chakrabarti P, et al. A study of hydrothermally grown ZnO nanorod-based metal-semiconductor-metal UV detectors on glass substrates. Nanomater Nanotechnol 2017;7. 1847980417702144.
[46] Wu Y, Dong B, Zhang J, Song H, Yan C. The synthesis of ZnO/$SrTiO_3$ composite for high-efficiency photocatalytic hydrogen and electricity conversion. Int J Hydrogen Energy 2018;43:12627–36.
[47] Baliga B. J. Power semiconductor devices (general engineering). PWS Pub. Co.; 1995.
[48] Li C, Dong S, Tang R, Ge X, Zhang Z, Wang C, et al. Heteroatomic interface engineering in MOF-derived carbon heterostructures with built-in electric-field effects for high performance Al-ion batteries. Energy Environ Sci 2018;11:3201–11.
[49] Shao K, Li F, Zhang G, Zhang Q, Maliutina K, Fan L, et al. Approaching durable single-layer fuel cells: promotion of electroactivity and charge separation via nanoalloy redox exsolution. ACS Appl Mater Interfaces 2019.